

## Approximating First Hitting Point Distribution in Milestoning for Rare Event Kinetics

## Approximating First Hitting Point Distribution in Milestoning for Rare Event Kinetics

Ru Wang,<sup>1</sup> Hao Wang\*,<sup>1</sup> Wenjian Liu,<sup>1</sup> and Ron Elber<sup>2,3</sup><sup>1)</sup>*Qingdao Institute for Theoretical and Computational Sciences,**Institute of Frontier and Interdisciplinary Science, Shandong University, Qingdao, Shandong 266237, P. R. China*<sup>2)</sup>*Oden Institute for Computational Engineering and Sciences,**University of Texas at Austin, Austin, Texas 78712, United States*<sup>3)</sup>*Department of Chemistry, University of Texas at Austin, Austin, Texas 78712, United States*

(\*Electronic mail: wanghaosd@sdu.edu.cn)

Milestoning is an efficient method for rare event kinetics calculation using short trajectory parallelization. Local kinetics between milestones are aggregated to compute the flux through the entire reaction space. In addition to the accuracy of force fields, the accuracy of Milestoning crucially depends on two factors: the initial distribution of the short trajectory ensemble and statistical adequacy of trajectory sampling. The latter can be improved by increasing the number of trajectories while the true initial distribution, i.e., first hitting point distribution (FHPD), has no analytic expression in the general case. Here, we propose two algorithms, local passage time weighted Milestoning (LPT-M) and Bayesian inference Milestoning (BI-M), to accurately and efficiently approximate FHPD for systems at equilibrium condition. Starting from equilibrium Boltzmann distribution on milestones, we calculate the proper weighting factor for equilibrium FHPD approximation and consequently for trajectory flux. The methods are tested on two model examples for illustration purpose. Both methods improve significantly over the widely used classical Milestoning method in terms of the accuracy of mean first passage time (MFPT). In particular, BI-M covers the directional Milestoning method as a special case in the deterministic Hamiltonian dynamics. LPT-M is especially advantageous in terms of computational costs and robustness with respect to the increasing number of intermediate milestones. Furthermore, a locally iterative correction algorithm for FHPD is proposed for exact MFPT calculation on the basis of LPT-M/BI-M, which is much cheaper than the exact Milestoning method.

## I. INTRODUCTION

Atomically detailed computer simulations are a useful tool to study thermodynamics and kinetics of molecular systems<sup>1</sup>. However, these calculations are expensive, and are not always feasible. The calculations of kinetics are particularly demanding since the samples are of complete reactive trajectories from reactants to products. This ensemble should be contrasted with the ensemble of configurations required for thermodynamic averages. Individual configurations are of orders of magnitude cheaper to sample than complete reactive trajectories.

Therefore, in the last two decades considerable efforts were invested to develop theories and algorithms for exact and approximate simulations of kinetics<sup>2</sup>. An attractive approach is based on the division of phase space into partitions or cells. We consider local kinetics between cells and the aggregation of the local kinetic results to compute the flux through the entire reaction space. Methods like Transition Interface Sampling<sup>3,4</sup> (TIS), Forward Flux Sampling<sup>5,6</sup> (FFS), Non-equilibrium Umbrella Sampling<sup>7</sup> (NEUS) and Milestoning<sup>8</sup> exploit the events of crossing boundaries between cells to estimate kinetic observables such as Mean First Passage Time (MFPT). We call the boundaries between cells milestones. Other approaches like Markov State Model<sup>9–11</sup> (MSM) or the Weighted Ensemble<sup>12,13</sup> (WE) approach, consider changes in the populations in the cells (not necessarily crossing the boundaries).

Milestoning provides a general mathematical framework for finite-state and continuous-time modeling of rare event kinetics. Many variants<sup>14–20</sup> have been developed since the first introduction of classical Milestoning<sup>8</sup> (CM). In addition to the accuracy of force fields, the accuracy of Milestoning crucially depends on two factors: the initial distribution of short trajectory ensemble and statistical adequacy of short trajectory sampling.

In this paper we consider the crossing point distribution on the milestone. We consider an exact definition and approximations. Each crossing point (a phase space configuration) has a weight of one for the long trajectory sampling. As such, the weight is nonuniform for sampling of a trajectory crossing. However, the entire weight of a trajectory including all crossing points must be one in the calculations of fluxes and kinetics. For a trajectory with multiple crossings, there are many ways of assigning weights to each crossing point. We may assign a weight of one for the first and zeros to the rest of crossing points. This choice leads to a distribution called the first hitting point distribution (FHPD). We denote it by  $f(x)$  where  $x$  is a phase space crossing point. The FHPD was discussed extensively in the context of Transition Path Theory<sup>21,22</sup> (TPT)

and was shown to provide the exact MFPT within the Milestoning theory<sup>23</sup>. FHPD has no analytic expression in the general case and needs to be approximated numerically.

In CM Boltzmann distribution (BD) constrained to a milestone is used as a rough approximation of FHPD in the canonical ensemble. When the distance between milestones is long and the potential energy slope is not steep, such an approximation is sound, as trajectories initiated from a milestone have sufficient time to relax to a local equilibrium before hitting a different one. However, for highly activated processes, milestones need to be placed closer, otherwise hitting events uphill in energy are challenging to sample. In this case, the discrepancy between BD and FHPD is appreciable. In directional Milestoning<sup>16</sup> (DiM) FHPD is obtained from a resampling procedure from an initial BD constrained to the milestone by removing those samples that are not real first hitting points. The selection is done by running trajectories from sampled configurations backward in time and checking if other re-crossing events are found before the trajectories cross another milestone. However, the removal of re-crossing trajectories results in considerable loss of statistics. In exact Milestoning<sup>17</sup> (ExM) FHPD is iteratively updated using BD as an initial guess. Under mild conditions, the iterations converge the distribution on milestones to FHPD<sup>24</sup>. However, the iterations are usually time consuming and more efficient approaches are desired.

The statistical adequacy of trajectory sampling is a trickier issue. However, an infinite MFPT output resulting from a disconnected Milestoning network clearly indicates an insufficient trajectory sampling. One possible scenario for this is the rare hitting events uphill in energy in an activated process. The biasing-and-reweighting method for trajectory sampling can be utilized to significantly enhance those otherwise rare transitions<sup>18,20</sup>.

In this paper, we propose two algorithms of approximating equilibrium FHPD. One is based on local passage time of a trajectory at crossing points. All configurations sampled on a milestone are retained. As a result, no statistics is lost. The other is based on Bayesian inference, which covers DiM as a special case in deterministic Hamiltonian dynamics but can also be applied to stochastic dynamics. Furthermore, a locally iterative correction algorithm for FHPD is proposed for exact MFPT calculation.

The remainder of this paper is organized as follows. First in Sec. II A we briefly review the Milestoning framework emphasizing on the effect of FHPD on MFPT calculation. Next, in Sec. II B we show how Milestoning can be combined with a long trajectory simulation to serve as the MFPT reference. In Sec. II C, we show the details of the algorithms. Finally, in Sec. III we illustrate the performance of our methods on two model examples.

## II. METHODS

### A. Milestoning Backdrop

We here only summarize the essential aspects of the Milestoning algorithm with the focus on illustrating how the FHPD affects the MFPT computation. Readers are referred to recent reviews for more detailed discussions of Milestoning algorithm<sup>25,26</sup> and software implementation<sup>27</sup>.

Consider a phase space of dimension  $\mathbb{R}^{6N}$  with  $N$  denoting the number of atoms. We are interested in the MFPT from a metastable region  $A$  (defined as the reactant state) to another disjoint metastable region  $B$  (defined as the product state) (cf. Fig. 1 (a)). When the transition from  $A$  to  $B$  is an activated process or dominated by slow diffusion on a rugged energy landscape, a straightforward molecular dynamics (MD) simulation is usually infeasible. However, to understand the key elements underlying Milestoning, it is useful to consider an infinitely long trajectory transiting back and forth between  $A$  and  $B$ . Based on which state ( $A$  or  $B$ ) the trajectory last visits, the path ensemble can be divided into two classes:  $A \rightarrow B$  and  $B \rightarrow A$ .

In Milestoning, the configuration space is partitioned into small compartments, and the interfaces between compartments are called milestones, which are denoted by  $\{M_1, M_2, \dots, M_n\}$ . The current state of the long trajectory is determined by the last milestone it crossed. As such, the path history in high-dimension phase space is mapped into a discretized milestone state space (Fig. 1 (b)), from which the transition probability  $K_{\alpha\beta}, \alpha, \beta \in \{M_1, M_2, \dots, M_n\}$ , between nearby milestones and the mean dwelling time  $t_\alpha$  on each milestone can be calculated. It has been shown that MFPT from  $A$  to  $B$  can be accurately calculated once  $\{K_{\alpha\beta}\}$  and  $\{t_\alpha\}$  of the partial path ensemble  $A \rightarrow B$  are known<sup>17,23</sup>.

In Milestoning calculations, both the transition probability  $K_{\alpha\beta}$  and mean dwelling time  $t_\alpha$  are calculated from the short trajectory ensemble initiated from a milestone, say  $\alpha$ , rather than resorting to brute-force long trajectory simulations. These short trajectories continue until they hit a different milestone  $\beta$  ( $\beta \neq \alpha$ ) for the first time. Short trajectories initiated from different milestones can run in trivial parallelization. This is why Milestoning is much more efficient than a brute-force long trajectory simulation. To be consistent with the long trajectory simulation, the true initial distribution of a short trajectory ensemble should be FHPD of partial path ensemble  $A \rightarrow B$ . First hitting points are phase space configurations that a trajectory arrives at a milestone for the first time after hitting another one.

Given FHPD of the partial path ensemble  $A \rightarrow B$  on the milestone  $\alpha$ ,  $f_\alpha(x_\alpha)$  ( $x_\alpha = (r_\alpha^{3N}, p_\alpha^{3N})$  denotes a phase space configuration on the milestone  $\alpha$ ), the transition probability  $K_{\alpha\beta}$  and the mean dwelling time  $t_\alpha$  are calculated as<sup>17</sup>

$$K_{\alpha\beta} = \int_\alpha dx_\alpha \int_\beta dx_\beta \int dt \cdot f_\alpha(x_\alpha) K(x_\alpha, x_\beta, t), \quad (1)$$

$$t_\alpha = \sum_{\beta \neq \alpha} \int_\alpha dx_\alpha \int_\beta dx_\beta \int dt \cdot t \cdot f_\alpha(x_\alpha) K(x_\alpha, x_\beta, t), \quad (2)$$

where  $K(x_\alpha, x_\beta, t)$  is the transition kernel starting from  $x_\alpha$  and ending at  $x_\beta$  during a time interval  $t$ . The concrete form of  $K(x_\alpha, x_\beta, t)$  depends on the equation of motion used to evolve the dynamics. In practice,  $K_{\alpha\beta} = n_{\alpha\beta}/n_\alpha$  where  $n_{\alpha\beta}$  out of  $n_\alpha$  trajectories initiated on the milestone  $\alpha$  first hit the milestone  $\beta$ , and  $t_\alpha = \sum_{i=1}^{n_\alpha} t_\alpha(i)/n_\alpha$  where  $t_\alpha(i)$  is the lifetime of the  $i$ th trajectory initiated on the milestone  $\alpha$ .

By the first-step analysis method, the MFPT,  $\tau_\alpha$ , from a certain milestone  $\alpha$  to the predefined product milestone  $\gamma$  satisfies a recurrence relation,

$$\tau_\alpha = t_\alpha + \sum_{\beta \neq \alpha} K_{\alpha\beta} \tau_\beta. \quad (3)$$

It has a simple physical explanation that the  $\alpha \rightarrow \gamma$  transition consists of a first step to a nearby milestone  $\beta$  and then a final  $\beta \rightarrow \gamma$  transition. Eq. (3) can be written in a more compact matrix equation form,

$$(\mathbf{I} - \mathbf{K}_A) \boldsymbol{\tau} = \mathbf{t}, \quad (4)$$

where  $\mathbf{I}$  is an  $n \times n$  identity matrix,  $\mathbf{K}_A$  is the transition probability matrix with element  $K_{\alpha\beta}$  except the row corresponding to the product state, and  $\boldsymbol{\tau}$  and  $\mathbf{t}$  are column vectors. By definition  $\tau_\gamma = 0$ , the  $\mathbf{K}_A$  matrix is imposed with absorbing boundary condition at the product state, i.e.,  $K_{A,\gamma\alpha} = 0$  for all  $\alpha \in \{M_1, M_2, \dots, M_n\}$ , and  $t_\gamma = 0$  to be consistent. This amounts to removing trajectories out of the system once they arrive at the product state, so as to only consider the partial path ensemble  $A \rightarrow B$ .

Alternatively, cyclic boundary condition can be set at the product state. Trajectories are re-injected into the reactant state  $\xi$  once they arrive at the product state  $\gamma$ , i.e.,  $K_{C,\gamma\alpha} = \delta_{\alpha\xi}$  for all  $\alpha \in \{M_1, M_2, \dots, M_n\}$  with  $\delta_{\alpha\xi}$  being the Kronecker delta function. The nonequilibrium stationary flux  $\{q_\alpha\}$  through each milestone obeys the eigenvalue equation

$$\mathbf{q}^t = \mathbf{q}^t \mathbf{K}_C. \quad (5)$$

The MFPT  $\tau_\xi$  is then calculated as

$$\tau_\xi = \sum_{\alpha} q_{\alpha} t_{\alpha} / q_{\gamma}. \quad (6)$$

The term  $q_{\alpha} t_{\alpha}$  is the stationary probability of last crossed milestone being  $\alpha$  in the partial path ensemble  $A \rightarrow B$ . Therefore Eq. (6) bears the meaning of "population over flux".

FHPD of the partial path ensemble  $A \rightarrow B$  plays an important role in MFPT calculation (Eqs. (4) and (6)) and has no analytic expression in the general case. Therefore it needs to be approximated numerically. In CM<sup>8</sup> it is roughly approximated by BD, while in ExM<sup>17</sup> it is iteratively corrected on the basis of CM by solving the self-consistent equation,

$$f_{\beta}^{(i+1)}(x_{\beta}) = \frac{1}{q_{\beta}^{(i)}} \sum_{\alpha \neq \beta} q_{\alpha}^{(i)} K_{\alpha\beta}^{(i)}(x_{\beta}), \quad (7)$$

where  $f_{\alpha}^{(i)}(x_{\alpha})$  is the approximate FHPD of the  $i$ th iteration and  $K_{\alpha\beta}^{(i)}(x_{\beta}) \equiv \int_{\alpha} dx_{\alpha} \int dt \cdot f_{\alpha}^{(i)}(x_{\alpha}) K(x_{\alpha}, x_{\beta}, t)$  is transition probability from milestone  $\alpha$  to  $x_{\beta}$ . Note that  $q_{\alpha}^{(i)}$ , as the solution of Eq. (5), is also a functional of  $\{f_{\alpha}^{(i)}(x_{\alpha})\}$  for all  $\alpha \in \{M_1, M_2, \dots, M_n\}$ .

## B. Milestoning Combined with a Long Trajectory Simulation as Reference

Long trajectory simulations provide an unbiased estimation FHPD and consequently exact  $K_{\alpha\beta}$  and  $t_{\alpha}$ . Transition events between nearby milestones are recorded for Milestoning calculation.

As mentioned above, it is important to only consider the partial path ensemble  $A \rightarrow B$  for exact MFPT calculation. Therefore, the boundary condition at the product state matters. It is convenient to set up either an absorbing boundary condition or a cyclic boundary condition at the product, so as to screen out the partial path ensemble  $A \rightarrow B$ . In practice, this can be achieved as follows. Draw a set of configurations in the reactant state in the canonical ensemble (a local equilibrium approximation at the reactant). For each configuration, draw initial velocities from Maxwell distribution and run a trajectory forward in time until it arrives at the product state. As such, these long trajectories constitute the partial path ensemble  $A \rightarrow B$ , from which  $\{K_{\alpha\beta}\}$  and  $\{t_{\alpha}\}$  are calculated.

The proper boundary condition at the product state is especially necessary when the configuration space partition is dense and trajectories have no sufficient time to relax, which is verified in our latter calculations.

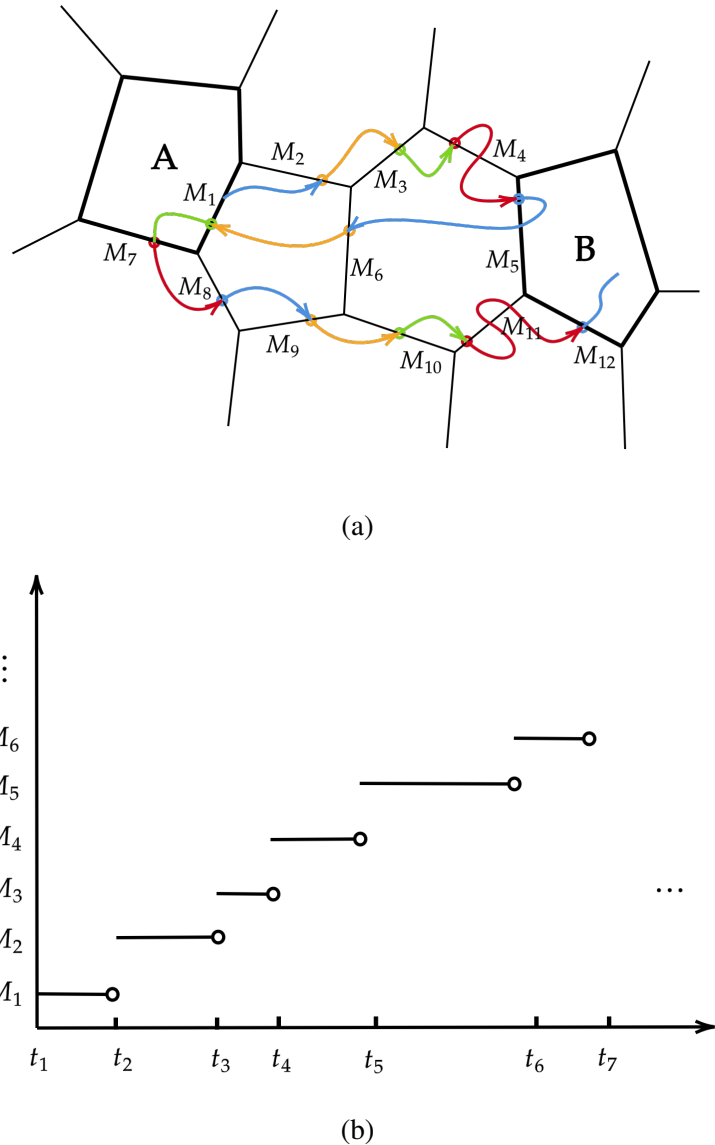


FIG. 1. (a) Schematic diagram of a long equilibrium trajectory transiting between *A* (reactant) and *B* (product). The current state of the trajectory is determined by the last milestone crossed and is coded in different colors (cycling through four colors). The first hitting points are marked out as circles. (b) The path history mapped into the discretized milestone state space.

### C. Approximating FHPD

The FHPD of partial path ensemble  $A \rightarrow B$  required for exact MFPT calculation is challenging to approximate, since it requires a backward tracing all the way to *A* or *B* to verify if a trajectory originates from *A*. Instead, we approximate the equilibrium FHPD consisting of path ensemble

$A \rightarrow B$  and  $B \rightarrow A$ . Even though it is not exact for MFPT calculation, the accuracy of predicted MFPT turns out to improve significantly compared to CM. Furthermore, we propose a locally iterative correction algorithm for FHPD for exact MFPT calculation, which is much cheaper than ExM.

### 1. Local Passage Time Weighting

We start from BD sampling on the milestone in the canonical ensemble and calculate the weighting factor needed for approximating equilibrium FHPD.

We first consider unconstrained sampling of BD on a milestone from a long equilibrium trajectory. In MD simulations, the time integration is discretized and configurations are saved every time step  $\Delta t$ . These configurations would not fall exactly on a milestone (a thickless interface) defined by  $M(r^{3N}) = m$ , where  $M(r^{3N})$  is a coarse function of Cartesian coordinates, e.g., interatomic distances, torsion angles etc., used to partition the configuration space. Instead we consider an infinitesimal interval  $[m, m + dM]$ . Whenever configurations fall into this interval, they are treated as falling on the milestone. All these configurations accumulated in  $[m, m + dM]$  together constitute BD on the milestone.

The number of configurations  $n_j$  falling into the interval  $[m, m + dM]$  during the  $j$ th crossing event is proportional to its local passage time  $dt_j$ ,  $n_j = dt_j/\Delta t$ . Or equivalently  $n_j$  is proportional to  $|v_j^\perp|^{-1}$  with  $v_j^\perp$  denoting the component of velocity normal to the milestone of crossing since  $dt_j = dM/|v_j^\perp|$ .

Assume after running a long equilibrium trajectory we observe four transition events in between milestones  $M_{a-1}$  and  $M_{a+1}$  passing through  $M_a$  (see Fig. 2). The transition probability is then estimated as  $K_{M_a M_{a+1}} = 2/4 = 0.5$  and  $K_{M_a M_{a-1}} = 2/4 = 0.5$  where each short piece of trajectories in between  $M_{a-1}$  and  $M_{a+1}$  is counted only once. However, when we sample from BD on  $M_a$  consisting of all crossing points, those short pieces of trajectories consisting of more points in  $[m, m + dM]$  will have a higher probability of being selected. The nonuniform (unnormalized) probability of the  $j$ th trajectory being selected from an initial BD sampling on  $M_a$  is  $p_j = \sum_l dt_{j,l} = \sum_l |v_{j,l}^\perp|^{-1}$ , where the summation is over all crossing events of the  $j$ th trajectory on  $M_a$ , and  $dt_{j,l}$  and  $v_{j,l}^\perp$  are the local passage time and the velocity component normal to  $M_a$  of the  $j$ th trajectory at the  $l$ th crossing, respectively. Since each short piece of trajectories in between  $M_{a-1}$  and  $M_{a+1}$  only contributes one first hitting point on  $M_a$ , the unbiased equilibrium FHPD obtained from an

initial BD sampling is estimated as  $f_{M_a}(x) = \frac{1}{Q} \sum_j \frac{1}{p_j} \delta(x - x_{FHP,j})$ , where the summation is over all short trajectories passing through  $M_a$ ,  $x_{FHP,j}$  is the first hitting point of the  $j$ th trajectory on  $M_a$ , and  $Q = \sum_j \frac{1}{p_j}$  is the normalization factor.

Based on the analysis above, we devise the local passage time weighted Milestoning (LPT-M) algorithm. In this algorithm, we construct an approximate equilibrium FHPD,  $f(x)$ , from configurations sampled in the canonical ensemble as is done in CM but considering nonuniform trajectory weights. The algorithm is summarized as follows,

- (1) Draw configurations on each milestone in the canonical ensemble by restrained MD simulations, e.g., adding a harmonic restraint  $\frac{1}{2}k(M(r^{3N}) - m)^2$ .
- (2) For each configuration, draw initial velocities from Maxwell distribution and run an unbiased trajectory forward in time until it hits a different milestone for the first time. Save the lifetime of the  $j$ th trajectory,  $t_j^f$ .
- (3) Reverse initial velocities and run an unbiased trajectory until it hits a different milestone for the first time. Save the lifetime from the initial configuration up to the last recrossing point of the  $j$ th trajectory,  $t_j^b$ . Optionally, save the configuration (and reversed velocity) at the last crossing point for  $f(x)$  estimation.
- (4) During the  $j$ th trajectory running in both forward and backward direction, record the velocity component perpendicular to the initial milestone at each crossing event,  $|v_{j,l}^\perp|$ .
- (5) Perform normal Milestoning analysis but now considering the nonuniform weight of each trajectory  $w_j = (\sum_l |v_{j,l}^\perp|^{-1})^{-1}$ , where the summation is over all crossing events in both forward and backward time integration of the  $j$ th trajectory. The transition probability and the mean dwelling time are calculated as  $K_{\alpha\beta} = \frac{\sum_{j \in (\alpha \rightarrow \beta)} w_j}{\sum_j w_j}$  and  $t_\alpha = \frac{\sum_j w_j (t_j^f + t_j^b)}{\sum_j w_j}$ .

We have used harmonic restraints to sample configurations in  $[m, m + dM]$  in (1) and used time reversibility for backward propagation in (3).

The local passage time weighting can also be justified in the Milestoning flux-probability language. Recall that the MFPT is calculated as "population over flux" (Eq. (6)). Consider now the milestone defined by  $M(r^{3N}) = m$  as the "reactant" and a virtual milestone defined by  $M(r^{3N}) = m + dM$  as the "product". For a phase space configuration  $x$  on the reactant milestone,

the MFPT is now just the local passage time  $t(x)$  and we have

$$t(x) = \frac{p(x)}{q(x)}, \quad (8)$$

where  $p(x)$  is the probability of last being at  $x$  and  $q(x)$  is the flux through  $x$ . The flux function  $q(x)$  is related to the FHPD  $f(x)$  by

$$q(x) = qf(x), \quad (9)$$

where  $q$  is the total flux passing through a milestone (Eq. (5)). Eq. (8) can be rewritten for a single trajectory only,  $q_j(x) = p_j(x)/t_j(x)$ . This expression suggests that in order to get the flux function (unnormalized FHPD) the probability should be weighted by the local passage time.

The weighting factor  $(\sum_l |v_l^\perp|^{-1})^{-1}$  was used in the context of transition path sampling from a single dividing surface by Hummer<sup>28</sup>. The single dividing surface is a separatrix located in the transition state in a two-state model. To generate an unbiased trajectory ensemble passing through the surface consistent with long equilibrium trajectories, each trajectory in the ensemble needs to carry a weight to be consistent with an equilibrium density on the surface. The transition path ensemble is then defined by those trajectories connecting reactant and product state considering proper weight. Milestoning network (Fig. 2) can be regarded as a union of "transition state model", in which a dividing surface (e.g.,  $M_a$ ) separating left milestone ( $M_{a-1}$ ) from right milestone ( $M_{a+1}$ ). An important difference from Hummer's method is that not only transition paths connecting reactant and product (e.g., red and blue trajectories) but also those returning back (e.g., orange and purple trajectories) contribute to the flux calculation.

## 2. Bayesian Inference

We now consider a continuous long equilibrium trajectory. In this case, the first hitting points are exactly on the milestone surface. Starting from BD constrained to a milestone, we construct another algorithm for approximating FHPD using the Bayesian inference,

$$P(x|FHP) = \frac{P_{eq}(x)P(FHP|x)}{P(FHP)}, \quad (10)$$

where  $P_{eq}(x) \sim e^{-\beta H(x)} \delta(M(r^{3N}) - m)$  is BD constrained to a milestone,  $P(FHP|x)$  is the conditional probability that a given phase space configuration is a first hitting point,  $P(FHP)$  can be regarded as a normalization constant and  $P(x|FHP)$  is the equilibrium FHPD we are looking for. Whether a given phase space configuration  $x$  is a first hitting point can be numerically verified by

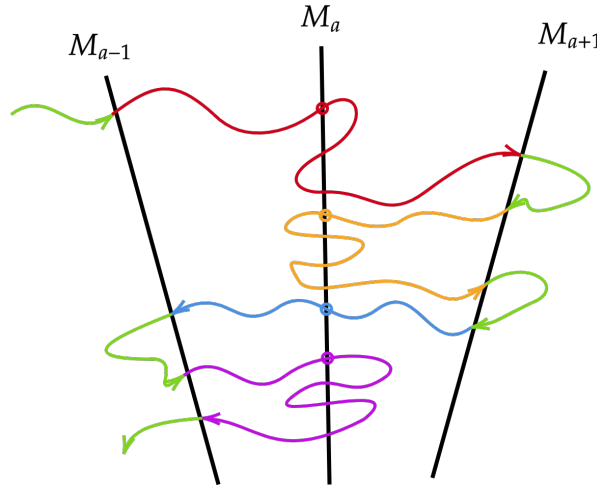


FIG. 2. Sketch of a long equilibrium trajectory passing through three consecutive milestones,  $M_{a-1}$ ,  $M_a$  and  $M_{a+1}$ . First hitting points on  $M_a$  are marked in circles.

running the trajectory backward in time starting from  $x$ , and check if the initial milestone is re-crossed. For the deterministic Hamiltonian dynamics  $P(FHP|x) = \delta_{x,x_{FHP}}$  and it naturally reduces to the DiM method<sup>16</sup>. For stochastic dynamics, such as Langevin dynamics,  $P(FHP|x)$  is no longer a Kronecker delta function and should be a probability ratio. This constitutes the following Bayesian inference Milestoning (BI-M) algorithm,

- (1) Draw configurations on each milestone in the canonical ensemble by constrained MD simulations.
- (2) For each configuration, draw initial velocities from Maxwell distribution.
- (3) Reverse the initial velocities and run  $n$  unbiased trajectories until they hit a different milestone for the first time. Count the number of times  $n_j$  of the initial phase space configuration being the real first hitting point. Estimate  $P(FHP|x_j) = n_j/n$ .
- (4) For those initial phase space configurations with non-zero  $P(FHP|x_j)$ , run an unbiased trajectory forward in time until it hits a different milestone for the first time. Record the trajectory lifetime  $t_j$ .
- (5) Perform normal Milestoning analysis but now considering the nonuniform weight of each trajectory  $w_j = z(r^{3N})^{-\frac{1}{2}}P(FHP|x_j)$  (or  $w_j = P(FHP|x_j)$ , see below). The transition probability and the mean dwelling time is calculated as  $K_{\alpha\beta} = \frac{\sum_{j \in (\alpha \rightarrow \beta)} w_j}{\sum_j w_j}$  and  $t_\alpha = \frac{\sum_j w_j t_j}{\sum_j w_j}$ .

The initial configurations sampled in (1) are assumed to be exactly on the milestone for  $P(FHP|x)$  estimation. This can be achieved either by imposing a rigid constraint  $\sigma(r^{3N}) = M(r^{3N}) - m = 0$  using Lagrange multiplier or SHAKE algorithm<sup>29</sup> or approximately by restrained MD simulations, e.g., adding a harmonic restraint  $\frac{1}{2}k(M(r^{3N}) - m)^2$ . When a rigid constraint is imposed<sup>30</sup>, the configurations sampled in (1) obey the distribution  $f(r^{3N}) \sim z(r^{3N})^{\frac{1}{2}} e^{-\beta U(r^{3N})} \delta(M(r^{3N}) - m)$  with the metric factor  $z(r^{3N}) = \sum_{i=1}^N \frac{1}{m_i} (\frac{\partial \sigma}{\partial \mathbf{r}_i})^2$ . In this case the weight factor in (5) should be  $w_j = z(r^{3N})^{-\frac{1}{2}} P(FHP|x_j)$ . When a harmonic restraint is used for initial sampling, the weight factor in (5) is simply  $w_j = P(FHP|x_j)$ .

### 3. Locally iterative correction

Due to the difference between equilibrium FHPD and FHPD of partial path ensemble  $A \rightarrow B$ , MFPT calculated with LPT-M and BI-M are not exact. In equilibrium condition first hitting points on a milestone would receive contributions from both path ensemble  $A \rightarrow B$  and  $B \rightarrow A$ . We here introduce a ratio function  $R_{A \rightarrow B}$  as an indicator, which measures the partial path ensemble  $A \rightarrow B$ 's contribution to the first hitting points on a milestone. When  $R_{A \rightarrow B}$  is lower than a certain threshold (e.g., 80%), it implies a potentially large discrepancy between the two FHPDs. Iterative correction (Eq. (7)) can then be specifically applied to those milestones where the FHPD discrepancy is large (i.e., locally iterative correction). As a result, the computational cost in each iteration can be greatly reduced compared to ExM.

We next illustrate how to compute  $R_{A \rightarrow B}$  on each milestone. Given a full transition probability matrix  $\mathbf{K}$  obtained from LPT-M or BI-M, we construct a reduced  $3 \times 3$  transition probability matrix  $\mathbf{K}^R$  with row 1 corresponding to the reactant milestone  $\xi$ , row 2 corresponding to a target intermediate milestone  $\alpha$  of which we want to calculate  $R_{A \rightarrow B}$ , and row 3 corresponding to the product milestone  $\gamma$ ,

$$\mathbf{K}^R = \begin{bmatrix} 0 & K_{12}^R & K_{13}^R \\ K_{21}^R & 0 & K_{23}^R \\ K_{31}^R & K_{32}^R & 0 \end{bmatrix}. \quad (11)$$

The matrix element, e.g.  $K_{12}^R$ , is just the commitment probability (or committor) that a trajectory initiated on the reactant milestone  $\xi$  will reach milestone  $\alpha$  first before the product milestone  $\gamma$ . The commitment probability corresponds to the splitting probability introduced by Onsager for ion-pair recombination<sup>31</sup>.

The calculation of committors in Milestoning is straightforward<sup>32</sup>. We first specify two milestones, say  $\alpha$  and  $\gamma$ , which serve as the end states. By the first-step analysis, it can be readily verified that the committor  $C_\beta$  of an arbitrary milestone  $\beta$ ,  $\beta \in \{M_1, M_2, \dots, M_n\}$ , first to  $\alpha$  rather than  $\gamma$  satisfies the following equation,

$$(\mathbf{I} - \tilde{\mathbf{K}})\mathbf{C} = \mathbf{e}_\alpha, \quad (12)$$

where  $\mathbf{I}$  is an  $n \times n$  identity matrix,  $\tilde{\mathbf{K}}$  is the full transition matrix except that two rows corresponding to milestones  $\alpha$  and  $\gamma$  are equal to zero, i.e.,  $\tilde{K}_{\alpha\beta} = 0$  and  $\tilde{K}_{\gamma\beta} = 0$  for all  $\beta \in \{M_1, M_2, \dots, M_n\}$ ,  $\mathbf{C}$  is a column vector of committors and  $\mathbf{e}_\alpha$  is a column vector of all zeros except the element corresponding to  $\alpha$  is equal to one. After solving Eq. (12) for  $\mathbf{C}$ , we have  $K_{12}^R = C_\xi$ . Repeat this process until we obtain all the matrix elements in  $\mathbf{K}^R$ .

We finally solve the eigenvalue equation  $\mathbf{q}^t = \mathbf{q}^t \mathbf{K}^R$  for equilibrium flux. The ratio of partial path ensemble  $A \rightarrow B$  on the target milestone  $\alpha$  is calculated as  $R_{A \rightarrow B}(\alpha) = q_1 K_{12}^R / q_2$ .

## D. Simulation Details

*Mueller's Potential.* The Mueller's potential is a 2D model system that has been used for benchmark test of kinetics<sup>14,15,20</sup>. We use Voronoi tessellation to partition the configuration space into small cells (Fig. 3). These cells are defined as

$$B_i = \{(\mathbf{r}, \mathbf{v}) \in \mathbb{R}^2 \times \mathbb{R}^2 : \|\mathbf{r} - \mathbf{r}_i\|_2 < \|\mathbf{r} - \mathbf{r}_j\|_2 \quad \text{for all } j \neq i\}. \quad (13)$$

The Voronoi centers  $\{\mathbf{r}_i\}$ , also called anchors, are placed along the minimum energy pathway (MEP) optimized by the zero-temperature string method<sup>33</sup>. We run underdamped Langevin dynamics

$$\dot{\mathbf{r}} = \mathbf{v}, \quad (14)$$

$$m\dot{\mathbf{v}} = -\frac{\partial U}{\partial \mathbf{r}} - \gamma \mathbf{v} + \eta, \quad (15)$$

using the Euler-Maruyama algorithm with the integration time step  $\Delta t = 10^{-4}$ , temperature  $k_B T = 10$ , friction coefficient  $\gamma = 10$  (or 100), and mass  $m = 1$ . The white noise  $\eta(t)$  is of mean zero and covariance  $\langle \eta_i(t) \eta_j(t') \rangle = 2\gamma k_B T \delta_{ij} \delta(t - t')$ . The energy barrier along the MEP is about  $10k_B T$ .

In LPT-M and CM method we use harmonic restraints to initially sample on each milestone, while in BI-M we use a rigid constraint for initial sampling. The rigid constraint can be easily

implemented in Voronoi tessellation by projecting initial velocities and forces at each time step onto the milestone hyperplane<sup>34</sup>. From each initially sampled phase space configuration we run backward in time ten times to estimate  $P(FHP|\mathbf{r}, \mathbf{v})$  in BI-M. The metric factor  $z(\mathbf{r})$  associated with the rigid constraint  $\sigma(\mathbf{r}) = (\mathbf{r} - \mathbf{r}_i)^2 - (\mathbf{r} - \mathbf{r}_j)^2 = 0$  is a constant. Therefore, the weighting factor in BI-M is simply  $w = P(FHP|\mathbf{r}, \mathbf{v})$ . Occasionally, the trajectory generated by forward and backward integration in time in LPT-M has zero crossings with the initial milestone. Such trajectories are discarded in Milestoning analysis. We run 1000 effective trajectories from each milestone. Ten independent simulations are run for each method (LPT-M, BI-M and CM). The average and standard deviation of MFPT are reported.

Locally iterative LPT-M (LiLPT-M) are performed as described in Sec. II C 3. All milestones with  $R_{A \rightarrow B}$  less than 80% participate in the iteration. Since the trajectory weight is nonuniform in LPT-M, when we resample on a milestone preparing for the next iteration, we have two choices: (i) resample trajectories by weight and then use them uniformly in the Milestoning analysis for the next iteration; (ii) Sample trajectories uniformly and then use them carrying weights in Milestoning analysis for the next iteration. These two ways are statistically equivalent giving the same unbiased estimation of the mean. We here choose (i) as the weighting factor needs no longer to be carried after the second iteration. Five independent simulations are run for error estimation. The transition probability and mean dwelling time of those milestones that do not participate in iteration are averaged first before iteration starts.

*Deca-alanine Unfolding in Vacuum.* The system is modeled as ACE-(Ala)<sub>10</sub>-NME (Fig. 7 (a)). The NAMD 2.14 program<sup>35</sup> and CHARMM36 force fields<sup>36</sup> are used for MD simulations. The integration time step is 1 fs. All atoms are included in nonbond interactions, i.e., no cutoff distance is set. The system runs in NVT ensemble using a Langevin thermostat at 600K with a friction constant  $1 \text{ ps}^{-1}$ . The end-to-end distance between two carbon atoms  $d_{CC}$  is used as the reaction coordinate to characterize the unfolding process. The reactant (folded) and product (fully extended) state are defined as  $d_{CC} = 13 \text{ \AA}$  and  $d_{CC} = 34 \text{ \AA}$ , respectively. 22 milestones uniformly separated by  $1 \text{ \AA}$  are placed along  $d_{CC}$  in  $[13 \text{ \AA}, 34 \text{ \AA}]$ .

We sample 400 configurations in the canonical ensemble at the reactant by restrained MD simulations, and run uninterrupted long trajectory ensemble from reactant to product. The time average is used as the MFPT reference.

In CM and LPT-M calculations we use restrained MD simulations with a force constant 12 kcal/mol/Å<sup>2</sup> to initially sample on each milestone. In BI-M calculation we use constrained MD

simulations for initial sampling on each milestone by fixing the positions of two carbon atoms at the end. Configurations are stored every 2 ps. In BI-M we run backward in time ten times from each initially sampled phase space configuration to estimate  $P(FHP|\mathbf{r}, \mathbf{v})$ . The metric factor  $z(\mathbf{r})$  associated with the rigid constraint  $\sigma(\mathbf{r}_{C_1}, \mathbf{r}_{C_2}) = \|\mathbf{r}_{C_1} - \mathbf{r}_{C_2}\|_2 - d_{CC}^0 = 0$  is a constant. The velocity component normal to a milestone is calculated using finite difference as  $|d_{CC}(t + \Delta t) - d_{CC}(t)|/\Delta t$  with  $t$  and  $t + \Delta t$  being the time moment right before and after the crossing, respectively. We run 400 effective trajectories from each milestone for Milestoning calculations. Five independent simulations are run for each method (LPT-M, BI-M and CM). The average and standard deviation of MFPT are reported.

### III. RESULTS AND DISCUSSIONS

In this section, we evaluate the performance of LPT-M and BI-M algorithms using two model systems, Mueller's potential and deca-alanine unfolding in vacuum.

The performance is evaluated from two perspectives: (i) the accuracy of predicted MFPT; (ii) the sensitivity of predicted MFPT with respect to the number of milestones. Since if true FHPD of the partial path ensemble  $A \rightarrow B$  is known, one can obtain exact MFPT at once. In this case, the configuration space should then be divided as fine as possible to achieve the highest efficiency without losing any accuracy. However, if the approximation is poor, one has to make the configuration space partition sparser, such that short trajectories have enough time to relax before they hit a different milestone.

#### A. Mueller's Potential

We first consider  $\gamma = 10$  which represents a low friction case. The inertia effect is significant. We place 24 anchors along the MEP (Fig. 3 (a) and Table S1). A milestone (cell interface) is indexed by two anchors defining it in Voronoi tessellation. The milestone (0, 1) and (22, 23) are defined as the reactant and the product state, respectively.

We first compare Milestoning analysis combined with a long trajectory simulation in two different boundary conditions at the product. One uses reflecting boundary condition (time length  $1 \times 10^7$ ), and the other uses cyclic boundary condition (2000 unidirectional transitions from reactant to product of total time length about  $1 \times 10^7$ ). We perform the Milestoning analysis by picking

up gradually increasing number of milestones ranging from 2 to 23 along the MEP (Fig. 4 (a) and Table S3). When only minimally two milestones (i.e., reactant and product) are reserved and all other intermediate milestones are omitted, both boundary conditions give exact MFPT since they both correspond to brute-force MD simulations from reactant to product. As intermediate milestones are gradually added on, MFPT prediction with the reflecting boundary condition starts deviating from the reference value and deviates most with 23 milestones, while the MFPT prediction with cyclic boundary condition remains accurate and stable. This confirms our statement that the true initial distribution of short trajectory ensemble required for exact MFPT calculation should be FHPD of the partial path ensemble  $A \rightarrow B$ .

We now compare LPT-M and BI-M with CM method in both dense (24 anchors) and sparse (12 anchors) partition of the configuration space (Fig. 5 (a)). The long trajectory simulation result with cyclic boundary condition is used as reference. The result shows that both LPT-M and BI-M improve significantly over CM. It is noteworthy that the LPT-M method approaches the accuracy limit of the long equilibrium trajectory simulation with reflecting boundary condition. In particular, LPT-M is less sensitive to the increasing number of intermediate milestones.

We also evaluate the computational costs in terms of the average number of force builds per milestone ( $N_{FB}$ ), as force evaluation is the most time-consuming part in MD simulations. The count of  $N_{FB}$  includes both the initial restrained sampling and free evolution of short trajectory ensemble. As is summarized in Table I, the LPT-M (BI-M) is about 1.5 (5.0) times as expensive as CM in both dense and sparse partition of the configuration space. However, it should be noted that the forward and backward evolution in LPT-M can run independently, leading to the same wall-clock time as CM.

The error of transition probability and mean dwelling time for milestones along the MEP are compared in Fig. S1 and S2, respectively. It can be seen that the error is mainly in the second half of MEP. It is noteworthy that milestones close to the reactant play more important roles in MFPT calculations, as their flux are orders of magnitude larger than those of milestones close to product (cf. Eq. (6)). By comparison with the  $R_{A \rightarrow B}$  profile (Fig. S3), we may draw the conclusion that under the current set-up when  $R_{A \rightarrow B}$  is lower than 80%, the discrepancy between equilibrium FHPD and FHPD of partial path ensemble  $A \rightarrow B$  becomes significant.

LiLPT-M and ExM are compared in Fig. 6. LiLPT-M converges faster and shows better stability in the iteration process. Since only partial milestones participate in the iteration, its computational cost increases at a lower rate.

TABLE I. Computational costs in terms of the number of force builds per milestone ( $N_{FB}$ ) obtained from CM, BI-M and LPT-M using 12 or 24 anchors along the minimum energy pathway on Mueller's potential.

$N_{FB}$ ( $\times 10^6$ )	$\gamma = 10$		$\gamma = 100$	
	12 anchors	24 anchors	12 anchors	24 anchors
CM	3.16	1.88	6.79	2.67
BI-M	17.04	8.18	22.62	8.45
LPT-M	5.56	2.88	12.66	4.44

We next consider  $\gamma = 100$  which represents a moderate friction case. The randomness of trajectories has increased compared to that of  $\gamma = 10$ . MFPT from a long trajectory simulation with reflecting boundary condition (time length  $5 \times 10^7$ ) and cyclic boundary condition (2000 unidirectional transitions from reactant to product of total time length about  $4 \times 10^7$ ) is shown in Fig. 4 (b). MFPT calculation with cyclic boundary condition still shows good robustness with respect to the increasing number of milestones. But MFPT calculation with the reflecting boundary condition is now less sensitive to the increasing number of milestones, since the velocity decorrelation is faster in  $\gamma = 100$  than in  $\gamma = 10$ . The deviation of MFPT with 23 milestones is about 1.5 times as large as the reference.

The MFPT accuracy of CM, BI-M and LPT-M in  $\gamma = 100$  are also compared (Fig. 5 (b)). At no surprise all three methods are now closer to the MFPT reference, among which LPT-M is still the most accurate one. In addition, all the three methods are now less sensitive to the increasing number of milestones, due to the faster velocity decorrelation. In Table I their computational costs are evaluated. BI-M is about 3.3 times as expensive as CM. The ratio is lower than that in  $\gamma = 10$ . The LPT-M is about 1.7 times as expensive as CM. The ratio is roughly the same as that in  $\gamma = 10$ .

## B. Deca-alanine Unfolding in Vacuum

MFPT of CM, BI-M and LPT-M from the folded state (reactant, Fig. 7 (a)) to each intermediate state until the fully extended state (product, Fig. 7 (a)) along the unfolding pathway is shown in Fig. 7 (b). Both BI-M and LPT-M improve over CM, and the LPT-M fits very well with the long trajectory ensemble reference in a low variance. Their computational costs in terms of the  $N_{FB}$  are summarized in Table. II. LPT-M is about 1.4 times as expensive as CM, while BI-M is about 3.3

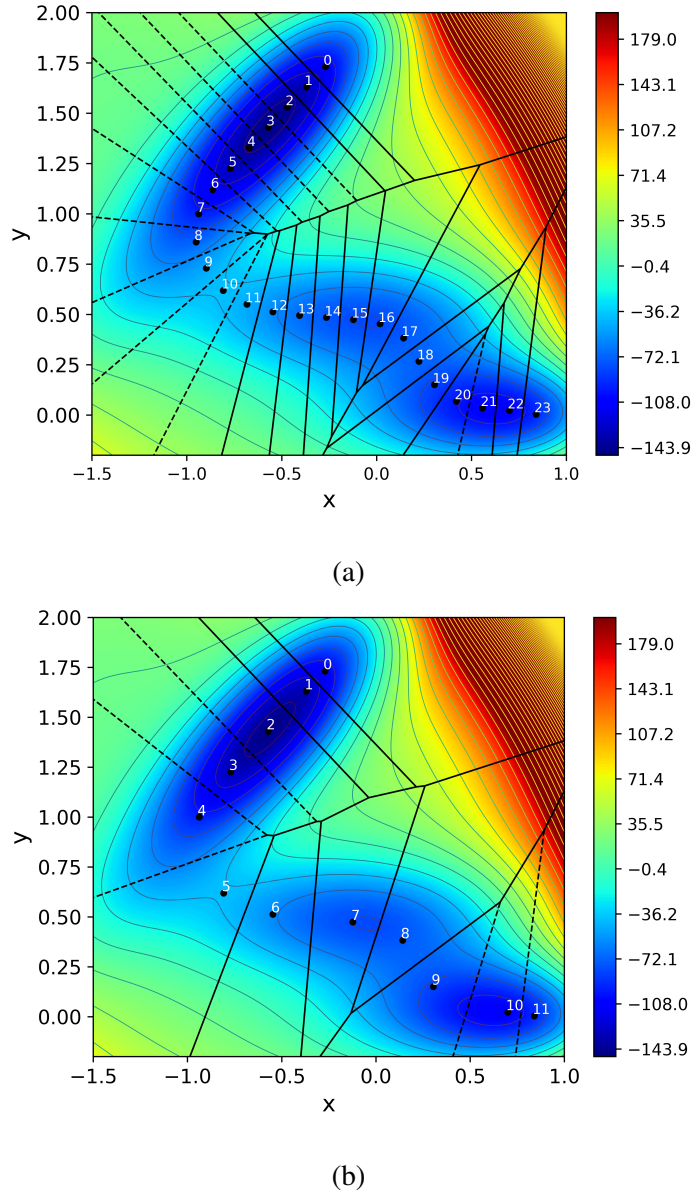


FIG. 3. Voronoi tessellation on the Mueller's potential with (a) 24 or (b) 12 anchors placed along the minimum energy pathway.

times as expensive as CM.

The error of transition probability and mean dwelling time for milestones along the unfolding pathway are shown in Fig. S4 and S5. The result shows that the transition probability error of LPT-M and BI-M is small on most milestones except the second to last. The  $R_{A \rightarrow B}$  profile remains close to 100% in the first half and falls quickly as approaching the product state (Fig. S6). In particular,  $R_{A \rightarrow B}$  of the second to last milestone falls below 40%, which raises a warning flag about potential discrepancy of two FHPDs.

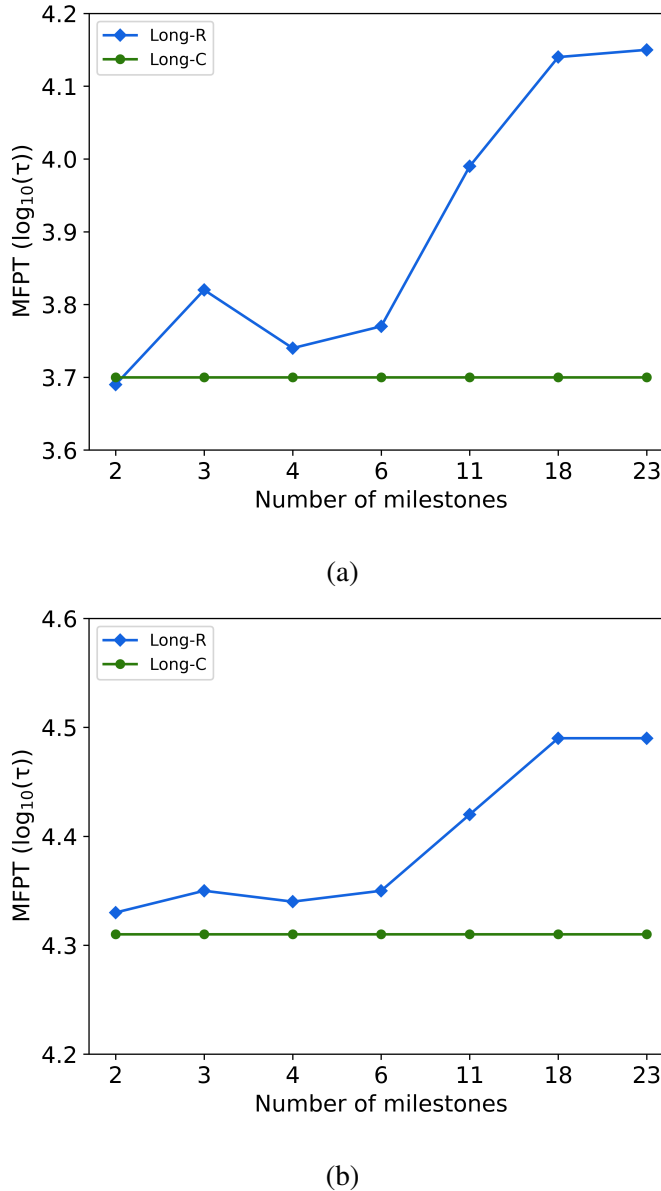


FIG. 4. MFPT calculations from a long trajectory simulation with (a)  $\gamma = 10$  or (b)  $\gamma = 100$  using reflecting boundary condition (Long-R) or cyclic boundary condition (Long-C) at product on Mueller's potential. Milestoning analysis is performed with increasing number of intermediate milestones.

#### IV. CONCLUSION

MFPT is the key kinetic output of Milestoning, whose accuracy crucially depends on FHPD. In order to obtain exact MFPT it is necessary to only consider the partial path ensemble  $A \rightarrow B$ . This has been extensively discussed in TPT<sup>21,22</sup>, NEUS<sup>7</sup>, FFS<sup>5,6</sup>, and trajectory tilting<sup>15</sup> approach. A convenient technique to screen out trajectories originating from reactant is to set up either absorb-

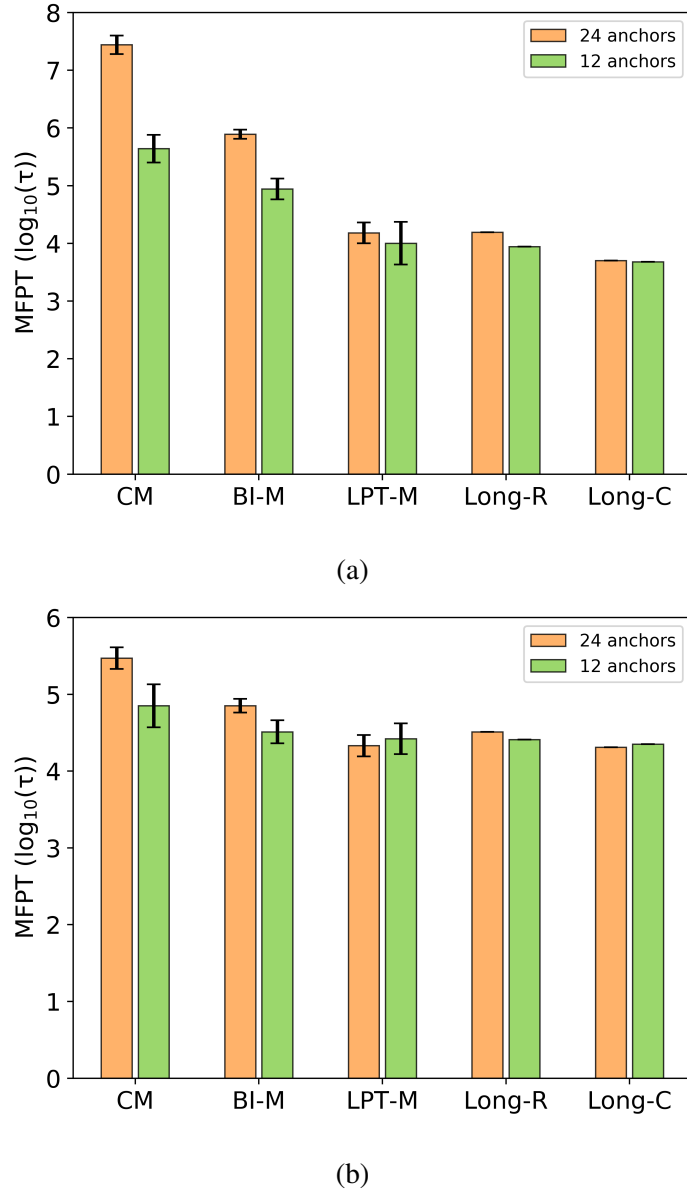


FIG. 5. MFPT calculations obtained from classical Milestoning (CM), BI-M, LPT-M, and a long trajectory simulation with reflecting boundary condition (Long-R) or cyclic boundary condition (Long-C). 12 or 24 anchors are placed along the minimum energy pathway on Mueller's potential. (a)  $\gamma = 10$ , (b)  $\gamma = 100$ .

ing or cyclic boundary condition at the product. This amounts to establishing a nonequilibrium condition. We here have developed two algorithms, LPT-M and BI-M, to approximate equilibrium FHPD on milestones. Even though the predicted MFPT are not exact, both methods improve significantly over CM. LPT-M is particularly preferable as its high accuracy approaching the limit of a long equilibrium trajectory simulation, better robustness with respect to the number of intermediate milestones and only a slight increase (about 50%) in computational costs with respect to

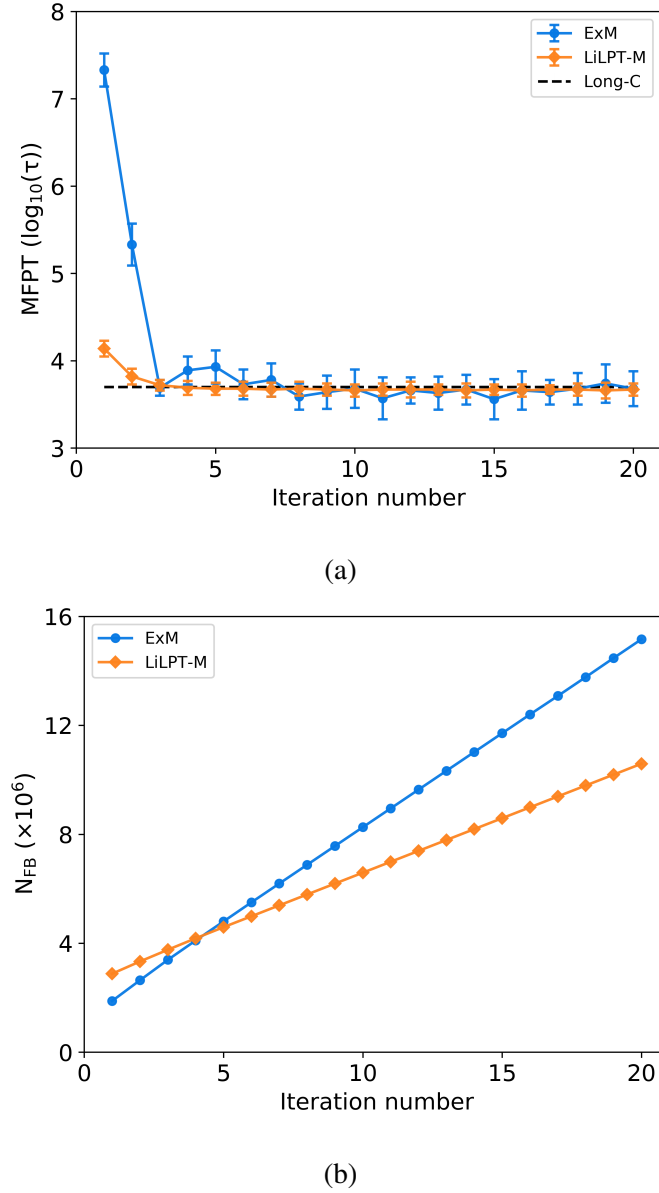


FIG. 6. The Mueller's potential is partitioned using 24 anchors along the minimum energy pathway. Dynamics is evolved with  $\gamma = 10$ . (a) MFPT from locally iterative LPT-M (LiLPT-M) and exact Milestoning (ExM) method are compared. MFPT from a long trajectory simulation with cyclic boundary condition at product is used as reference. (b) Computational costs in terms of the number of force builds per milestone  $N_{FB}$  for LiLPT-M and ExM.

CM. Note that its wall-clock time is actually the same as CM, since the forward and backward trajectory in LPT-M can run in parallel. Furthermore, we introduce a ratio function which can be used to indicate potential discrepancy between equilibrium FHPD and FHPD of the partial path ensemble  $A \rightarrow B$  on milestones. Based on this, a local iteration algorithm is proposed for exact

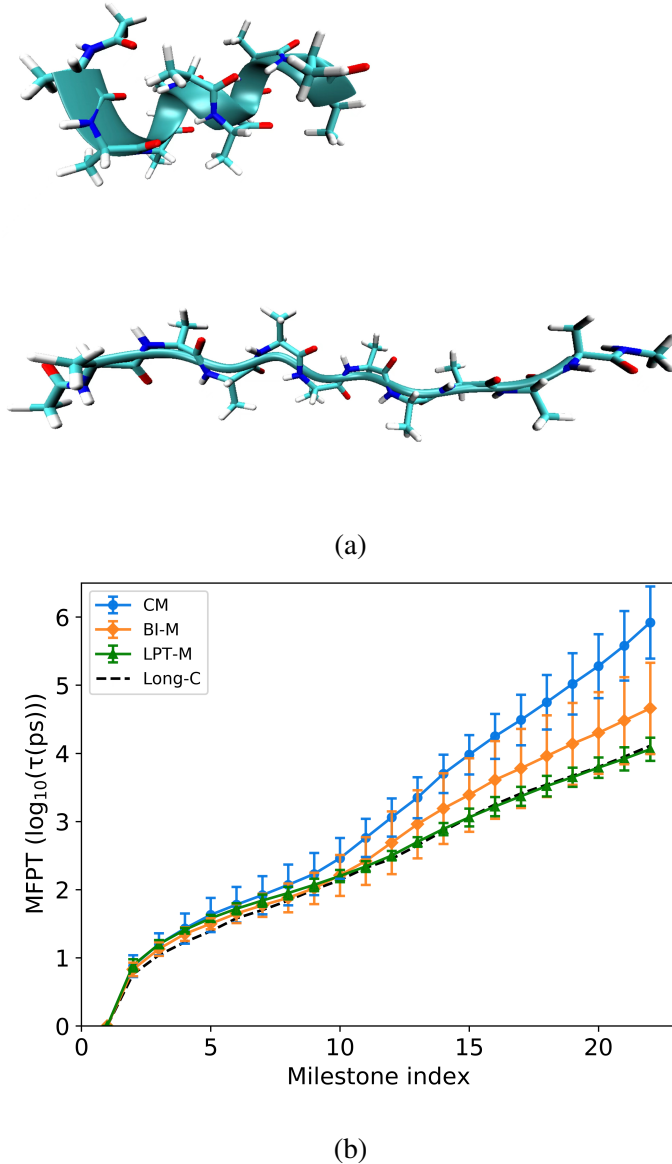


FIG. 7. (a) The folded and fully extended structure of deca-alanine. (b) MFPT of CM, LPT-M and BI-M from the folded state (milestone 1) to each intermediate milestone until the fully extended one (milestone 22) along the deca-alanine unfolding process in vacuum. MFPT from a long trajectory ensemble with cyclic boundary condition (Long-C) serves as reference.

MFPT calculation on the basis of LPT-M/BI-M and has a lower computational cost than ExM, in which all milestones participate in iteration without selection.

TABLE II. The average number of force builds per milestone ( $N_{FB}$ ) of CM, LPT-M and BI-M in deca-alanine unfolding in vacuum.

	CM	LPT-M	BI-M
$N_{FB}$ ( $\times 10^6$ )	1.1	1.5	3.6

## ACKNOWLEDGMENTS

This work was supported by the Qilu Young Scholars Program of Shandong University.

## DATA AVAILABILITY STATEMENT

The data that support the findings of this study are available within the article and its supplementary material.

## CONFLICTS OF INTEREST

There are no conflicts to declare.

## SUPPORTING INFORMATION

Anchor positions on Mueller's potential in Fig. 3, milestone corresponding list in Fig. 4, the error plot of transition probability and mean dwelling time and the ratio function  $R_{A \rightarrow B}$  profile along the reaction pathway in Mueller's potential and deca-alanine unfolding process.

## REFERENCES

- <sup>1</sup>D. Frenkel and B. Smit, *Understanding molecular simulation: From algorithms to applications*, 2nd ed. (Academic Press, 2002).
- <sup>2</sup>R. Elber, D. E. Makarov, and H. Orland, *Molecular dynamics in condensed phases: Theory, simulations, and analysis* (John Wiley and Sons: New Jersey, 2020).
- <sup>3</sup>T. S. van Erp, D. Moroni, and P. G. Bolhuis, *The Journal of Chemical Physics* **118**, 7762 (2003).
- <sup>4</sup>T. S. van Erp and P. G. Bolhuis, *Journal of Computational Physics* **205**, 157 (2005).
- <sup>5</sup>R. J. Allen, D. Frenkel, and P. R. ten Wolde, *The Journal of Chemical Physics* **124**, 194111 (2006).
- <sup>6</sup>R. J. Allen, C. Valeriani, and P. R. ten Wolde, *Journal of Physics: Condensed Matter* **21**, 463102 (2009).
- <sup>7</sup>A. Dickson, A. Warmflash, and A. R. Dinner, *The Journal of Chemical Physics* **131**, 154104 (2009).
- <sup>8</sup>A. K. Faradjian and R. Elber, *The Journal of Chemical Physics* **120**, 10880 (2004).
- <sup>9</sup>J.-H. Prinz, H. Wu, M. Sarich, B. Keller, M. Senne, M. Held, J. D. Chodera, C. Schütte, and F. Noé, *The Journal of Chemical Physics* **134**, 174105 (2011).
- <sup>10</sup>G. R. Bowman, V. S. Pande, and F. Noé, *An introduction to markov state models and their application to long timescale molecular simulation* (Springer, 2014).
- <sup>11</sup>B. E. Husic and V. S. Pande, *Journal of the American Chemical Society* **140**, 2386 (2018).
- <sup>12</sup>G. A. Huber and S. Kim, *Biophysical Journal* **70**, 97 (1996).
- <sup>13</sup>B. W. Zhang, D. Jasnow, and D. M. Zuckerman, *The Journal of Chemical Physics* **132**, 054107 (2010).
- <sup>14</sup>E. Vanden-Eijnden and M. Venturoli, *The Journal of Chemical Physics* **130**, 194101 (2009).
- <sup>15</sup>E. Vanden-Eijnden and M. Venturoli, *The Journal of Chemical Physics* **131**, 044120 (2009).
- <sup>16</sup>P. Májek and R. Elber, *Journal of Chemical Theory and Computation* **6**, 1805 (2010).
- <sup>17</sup>J. M. Bello-Rivas and R. Elber, *The Journal of Chemical Physics* **142**, 094102 (2015).
- <sup>18</sup>G. Grazioli and I. Andricioaei, *The Journal of Chemical Physics* **149**, 084103 (2018).
- <sup>19</sup>D. Ray and I. Andricioaei, *The Journal of Chemical Physics* **152**, 234114 (2020).
- <sup>20</sup>H. Wang and R. Elber, *The Journal of Chemical Physics* **152**, 224105 (2020).
- <sup>21</sup>W. E and E. Vanden-Eijnden, *Journal of Statistical Physics* **123**, 503 (2006).
- <sup>22</sup>W. E and E. Vanden-Eijnden, *Annual Review of Physical Chemistry* **61**, 391 (2010).

<sup>23</sup>E. Vanden-Eijnden, M. Venturoli, G. Ciccotti, and R. Elber, *The Journal of Chemical Physics* **129**, 174102 (2008).

<sup>24</sup>D. Aristoff, J. M. Bello-Rivas, and R. Elber, *Multiscale Modeling & Simulation* **14**, 301 (2016).

<sup>25</sup>R. Elber, *Annual Review of Biophysics* **49**, 69 (2020).

<sup>26</sup>R. Elber, A. Fathizadeh, P. Ma, and H. Wang, *WIREs Computational Molecular Science* **11**, e1512 (2021).

<sup>27</sup>A. E. Cardenas, A. Hunter, H. Wang, and R. Elber, *Journal of Chemical Theory and Computation* **18**, 6952 (2022).

<sup>28</sup>G. Hummer, *The Journal of Chemical Physics* **120**, 516 (2004).

<sup>29</sup>J.-P. Ryckaert, G. Ciccotti, and H. J. Berendsen, *Journal of Computational Physics* **23**, 327 (1977).

<sup>30</sup>M. Sprik and G. Ciccotti, *The Journal of Chemical Physics* **109**, 7737 (1998).

<sup>31</sup>L. Onsager, *Phys. Rev.* **54**, 554 (1938).

<sup>32</sup>R. Elber, J. M. Bello-Rivas, P. Ma, A. E. Cardenas, and A. Fathizadeh, *Entropy* **19** (2017).

<sup>33</sup>W. E, W. Ren, and E. Vanden-Eijnden, *Phys. Rev. B* **66**, 052301 (2002).

<sup>34</sup>J. Bajars, J. Frank, and B. Leimkuhler, *The European Physical Journal Special Topics* **200**, 131 (2011).

<sup>35</sup>J. C. Phillips, D. J. Hardy, J. D. C. Maia, J. E. Stone, J. a. V. Ribeiro, R. C. Bernardi, R. Buch, G. Fiorin, J. Hénin, W. Jiang, R. McGreevy, M. C. R. Melo, B. K. Radak, R. D. Skeel, A. Singhary, Y. Wang, B. Roux, A. Aksimentiev, Z. Luthey-Schulten, L. V. KalÃl', K. Schulten, C. Chipot, and E. Tajkhorshid, *The Journal of Chemical Physics* **153**, 044130 (2020).

<sup>36</sup>J. Huang, S. Rauscher, G. Nawrocki, T. Ran, M. Feig, B. L. de Groot, H. Grubmüller, and A. D. MacKerell Jr, *Nature Methods* **14**, 71 (2017).

TOC

